# The sensitivity of simulated competition between different plant functional types to sub-grid-scale representation of vegetation in a land surface model

**R. K. Shrestha[1], V. K. Arora[1] and J. R. Melton[2]**

[1]Canadian Centre for Climate Modelling and Analysis, Environment and Climate Change Canada, University of Victoria, Victoria, BC, V8W 2Y2, Canada

[2]Climate Research Division, Environment and Climate Change Canada, Downsview, Ontario, Canada

*Correspondence to: V. K. Arora (Vivek.Arora@ec.gc.ca)*



This article has been accepted for publication and undergone full peer review but has not been through the copyediting, typesetting, pagination and proofreading process which may lead to differences between this version and the Version of Record. Please cite this article as doi: 10.1002/2015JG003234

**Abstract**

The Canadian Land Surface Scheme (CLASS) coupled to the Canadian Terrestrial Ecosystem Model (CTEM) is used to simulate competition between the model's seven non-crop plant functional types (PFTs) for available space. Our objective is to assess if the model is successfully able to reproduce the observed mix of PFTs and their fractional coverages, and to what extent the simulated competition is affected by the manner in which the sub-grid scale variability of vegetation is represented. The model can be run either in a composite (single tile) configuration, where structural vegetation attributes of PFTs are aggregated for use in grid-averaged energy and water balance calculations, or a mosaic (multiple tiles) configuration, where separate energy and water balance calculations are performed for each PFT. The model realistically simulates the fractional coverages of trees, grasses and bare ground, as well as that of individual tree and grass PFTs and their succession patterns. Our results show that the model is not overly sensitive to the manner in which sub-grid scale variability of vegetation is represented. Of the seven sites chosen across the globe to illustrate the difference between the two configurations, the simulated fractional coverage of PFTs are generally very similar (root mean square difference, RMSD, < 5 %) between the composite and mosaic configurations at locations characterized by low heterogeneity (e.g. Amazonia, Vancouver Island, and the Tibetan Plateau), whereas at locations characterized by high heterogeneity (e.g. India, South Sudan and California), the two configurations yield somewhat different results (RMSD > 5 %).

## 1. Introduction

The dynamics of vegetation, which contributes to large sources of uncertainty in Earth system models (Purves and Pacala, 2008), is driven by several interacting factors including climate, disturbance and the biotic environment of vegetation. Understanding and modeling how the various biotic and abiotic factors interact and affect plant coexistence and competition is complicated (Anand, 2000;Berger et al., 2008). It is even more difficult to realistically represent the multi-dimensional behaviour of vegetation in Earth system models that treat vegetation as a dynamic component of the climate system (Lienard et al., 2014;Kutzbach et al., 1996). The dynamic behaviour of vegetation can be described by two aspects: the structural changes and the areal coverage changes. The structural dynamics include changes in vegetation height, leaf area index (LAI), rooting depth and canopy mass typically on seasonal to decadal time scales (Kramer and Kozlowski, 1979). Areal vegetation dynamics has slower time scales than the structural vegetation dynamics typically operating on decadal to centennial time scales (Ritchie and MacDonald, 1986). Areal dynamics includes succession, colonization and competition between different vegetation types for space which change the areal extent of vegetation.

Plants compete for above-ground light/radiation resources by changing their height and LAI (Purves and Pacala, 2008) and by changing their rooting structure and depth to access below-ground water and nutrients (Daufresne and Hedin, 2005). With these structural changes plants capture both above- and below-ground resources to increase their areal expanse and overtop their neighbours. In the horizontal direction, plants compete for space, which determines competitive exclusion and/or coexistence of a plant functional type (PFT) in a community ( Begon et al., 1986; Arora and Boer, 2006;Xiang and Xiaodong, 2014). The areal plant dynamics are also influenced by disturbances (Chambers et al., 2013). For instance,

environmental disturbances like fire reduce the density of plants making the burnt area available for re-occupancy by other plants (Curtis and Partch, 1948;Xie et al., 2013;Bond-Lamberty et al., 2009).

A broad spectrum of theoretical and phenomenological approaches have been established to study competition and co-existence of plants, ranging from the use of simple analytical techniques such as the Lotka–Volterra (LV) predator-prey equations (Begon et al., 1986) to a very detailed gap models (e.g. Bugmann, 2001) and hybrid approaches like the one used in the ecosystem demography (ED) model that attempt to implement gap dynamics within the framework of traditional ecosystem models (Moorcroft et al., 2001). The LV equations that were originally designed for simulating predator–prey relationship have been used in several terrestrial ecosystem models e.g. TRIFFID (Cox, 2001); USCM (Brentnall et al., 2005); CTEM (Arora and Boer, 2006), and by Fernandez-Illescas and Rodriguez-Iturbe (2003). Gap models simulate vegetation dynamics at the scale of an individual tree and thus are computationally expensive to run, making them more suitable for local or regional scale applications. Approaches simpler than the use of the LV equations also exist where the best performing PFT, on the basis of its net primary productivity (NPP), is assumed to occupy the largest fraction (e.g. Sitch et al., 2003).

The classical LV equations when used to simulate competition between PFTs suffer from the limitation of an amplified expression of dominance in that the most dominant PFT ends up occupying a large fraction of a grid cell, allowing little coexistence of PFTs. This limitation of the LV equations, when used in their classical format, is discussed in detail by Arora and Boer (2006) who also modified the classical LV equations to allow for coexistence of PFTs.

Here, we test the performance of the modified version of LV equations, following Arora and Boer (2006), to simulate competition between PFTs at seven selected locations across the globe using a new version of the CLASS-CTEM modelling framework (Canadian Land Surface Scheme version 3.6 coupled to Canadian Terrestrial Ecosystem Model version 2.0, Melton and Arora (2016)). Amongst other improvements, the modelling framework can be run in either the composite (single tile) or the mosaic (multiple tiles) configuration (Melton and Arora, 2014) – the two approaches to represent the sub-grid scale variability of vegetation. The two configurations of representing sub-grid scale variability of vegetation differ in the manner in which energy and water balance calculations are performed and the choice of either in turn also affects the simulated carbon balance and the competition between PFTs. In the composite configuration, the structural vegetation attributes (including LAI, vegetation height, and rooting depth) of PFTs that exist in a grid cell are averaged in proportion to their fractional coverages and then used in the grid-averaged energy and water balance calculations. As a result the entire grid cell is characterized by a surface physical environment (including soil temperature, soil moisture, fractional snow cover, and net radiation) that is common to all PFTs. In contrast, in the mosaic configuration a grid cell is split into multiple tiles representing individual PFTs for which energy and water balance calculations are performed separately. Each PFT tile in this case is characterized by a surface physical environment that is the result of its PFT's structural vegetation attributes interacting with the driving climate data and the carbon balance in individual tiles evolves independently of the other tiles. Since energy and water balance calculations are performed separately for all PFTs present in a grid cell in the mosaic configuration it is inherently more expensive than the composite configuration.

Previously, Li and Arora (2012) have investigated the impact of using composite versus

mosaic approaches on various aspects of the simulated energy and carbon balance at selected individual sites, and Melton and Arora (2014) have compared the effect of using these two approaches on the simulated carbon balance at the global scale, using earlier versions of the CLASS-CTEM modelling framework. Li and Arora (2012) found that the simulated energy balance is not extremely sensitive to the representation of sub-grid scale variability of vegetation; they found differences in energy fluxes that were generally less than 5%. Both studies found that simulated carbon balance is sensitive to the representation of the sub-grid scale variability of vegetation, with differences in simulated carbon pools and fluxes greater than 30%. Both Li and Arora (2012) and Melton and Arora (2014) studies, however, used specified fractional coverage of PFTs and competition between PFTs was not simulated. More recently, Melton and Arora (2016) have evaluated the performance of the modified version of the LV equations at the global scale by comparing simulated geographical distribution of CTEM's PFTs with observation-based estimates. They, however, used only the composite approach to represent sub-grid scale variability of vegetation and did not assess the effect of using the mosaic approach. Melton and Arora (2016) also did not assess the successional behaviour of vegetation.

Here, we assess the sensitivity of the simulated competition between PFTs, based on the modified version of the LV equations, to the representation of sub-grid scale variability of vegetation. Our objective is to assess if the new CLASS-CTEM modeling framework successfully reproduces the observation-based mix of PFTs and their fractional coverages at the selected seven sites, and to what extent these results are affected by the use of composite versus the mosaic configurations. The results provide insight into the worthiness of the additional computational expense of the mosaic approach in so far as the goal is to realistically simulate observed mix of PFTs and their fractional coverages. Finally, we also

assess the simulated successional dynamics of vegetation against available empirical evidence.

Section 2 of this paper briefly describes the CLASS-CTEM modeling framework, followed by the details of experimental set up and observation dataset in section 3. The results from the selected study sites are presented and discussed in section 4 and summary and conclusions are described in section 5.

## 2. Model description

Version 1.0 of the CTEM, which uses prescribed fractional coverage of PFTs and does not allow competition between them, is the terrestrial carbon cycle component of the second generation Canadian Earth System Model (CanESM2) (Arora et al., 2011) where it is coupled to version 2.7 of the CLASS. Version 2 of CTEM (Melton and Arora, 2016), which dynamically simulates fractional coverage of PFTs, used here is coupled to the CLASS version 3.6 (Verseghy, 2012). CTEM models terrestrial ecosystem processes for seven non-crop and two crop PFTs (see Table 1), by tracking the flow of carbon through three living vegetation components (leaves, stem and roots) and two dead carbon pools (litter and soil). The amount of carbon in these five carbon pools is simulated prognostically as a function of driving climate and atmospheric $CO_2$ concentration. The amount of carbon in the leaves, stem and root components is used to determine structural attributes of vegetation; LAI is calculated from leaf biomass using PFT-dependent specific leaf area (SLA) which determines the area of leaves that can be constructed with a given amount of leaf biomass, vegetation height is calculated based on stem biomass for tree PFTs and LAI for grass PFTs, and rooting depth is calculated based on root biomass. Parameterizations of various terrestrial ecosystem processes modelled in CTEM are described in various papers; these include photosynthesis,

autotrophic and heterotrophic respiration (Arora, 2003); phenology, carbon allocation, biomass turnover of leaves, stem and root components, and conversion of biomass to structural attributes (Arora and Boer, 2005b); dynamic root distribution (Arora and Boer, 2003); and fire (Arora and Boer, 2005a). Version 2 of CTEM (Melton and Arora, 2016) used here models these processes and also includes competition for space, based on the modified version of LV equations following Arora and Boer (2006), between its seven non-crop PFTs and this is the focus of our study.

CLASS models the land surface energy and water balance and calculates liquid and frozen soil moisture, and soil temperature for three soil layers (with thicknesses 0.1, 0.25 and 3.75 m). It performs energy and water balance calculations for four PFTs (needleleaf trees, broadleaf trees, crops and grasses) which map directly to the nine PFTs represented in CTEM as shown in Table 1. Needleleaf trees in CTEM are divided into their deciduous and evergreen versions for which terrestrial ecosystem processes are modelled separately, broadleaf trees are divided into their cold and drought deciduous and evergreen versions, and crops and grasses are divided into $C_3$ and $C_4$ versions based on their photosynthetic pathways.

CLASS can operate on its own and in this mode it simulates energy and water balance based on specified structural attributes of vegetation (including LAI, vegetation height, canopy mass and rooting depth). CTEM, however, cannot operate in the absence of CLASS. When coupled to CLASS, CTEM uses soil moisture, soil temperature and net shortwave radiation calculated by CLASS and in turn provides it dynamically simulated values of structural attributes of vegetation. Use of CTEM thus makes vegetation a dynamic component in CLASS. Combined, CLASS and CTEM simulate the fluxes of energy, water and $CO_2$ at the land-atmosphere boundary. CLASS operates at a time step of 30 minutes or shorter. CTEM

simulates photosynthesis and calculates the associated canopy conductance values at the time step of CLASS, but other terrestrial ecosystem processes in CTEM are simulated at a daily time step. Coupled CLASS and CTEM can be operated in the composite or mosaic configuration.

Competition in CTEM is parameterized on the basis of a modified version of the LV equations as presented in Arora and Boer (2006). The approach is described in detail by Melton and Arora (2016) who test the performance of the modified LV equations at the global scale using the composite approach and also document version 2.0 of CTEM.

The approach used for modelling competition in CTEM is briefly described here. Consider a grid cell in which two PFTs can exist. The PFTs are ranked in order of their superiority, as explained later, so PFT 1 (e.g. a tree PFT) is considered superior to and can invade PFT 2 (e.g. a grass PFT). If $f_i$ is the fraction coverage of PFT *i* then $f_1 + f_2 + f_B = 1$, where $f_B$ is the bare fraction in the grid cell. The rate of change of the fractional coverages of the two PFTs and bare fraction, for this example, are given by,

$$\frac{df_1}{dt} = c_1 f_1^{\beta}(1 - f_1) - m_1 f_1 \quad (1)$$

$$\frac{df_2}{dt} = c_2 f_2^{\beta}(1 - f_1 - f_2) - c_1 f_1^{\beta} f_2 - m_2 f_2 \quad (2)$$

$$\frac{df_B}{dt} = -c_1 f_1^{\beta} f_B - c_2 f_2^{\beta} f_B + m_1 f_1 + m_2 f_2 \quad (3)$$

where $c_1$, $c_2$ and $m_1$, $m_2$ are the colonization and mortality rates for PFT 1 and PFT 2, respectively. Colonization and mortality rates cannot be negative. In equation (1), PFT 1 is able to expand into the fraction covered by PFT 2 and the bare fraction. In equation (2), PFT 2 is able to expand only into the bare fraction. PFT 2 cannot expand into the fraction covered by PFT 1 because it is ranked lower than PFT 1. The exponent β ($0 \leq \beta \leq 1$), an empirical parameter, controls the behaviour of the LV equations. For β = 1, the equations take the classical form of the LV equations. The equilibrium fractional coverages for PFT 1 and 2 and bare fraction for this classical form of the LV equations, denoted by $\tilde{f}_i$ , are given by,

$$\tilde{f}_1 = \max\left\{\left(\frac{c_1 - m_1}{c_1}\right), 0\right\} \quad (4)$$

$$\tilde{f}_2 = \max\left\{\left(\frac{(c_2 - m_2) - \left(1 + \frac{c_2}{c_1}\right)(c_1 - m_1)}{c_2}\right),\ 0\right\} \quad (5)$$

$$\tilde{f}_B = \frac{(m_1\tilde{f}_1 + m_2\tilde{f}_2)}{(c_1\tilde{f}_1 + c_2\tilde{f}_2)} \quad (6)$$

The classical LV equations with β = 1 suffer from two limitations. First, if $f_i$ is initially zero then in equations (1) and (2) $\frac{df_i}{dt} = 0$ and a PFT cannot expand, implying that a minimum seeding fraction is always required. Second, in equation (5) as long as ($c_1$–$m_1$) is greater than ($c_2$–$m_2$) then the equilibrium solution for $f_2$ will always be zero and PFT 2 will not be able to coexist with PFT 1. When $\beta = 0$, equations (1) - (3) represent the modified version of the LV equations as used by Arora and Boer (2006). The equilibrium fractional coverages for PFT 1 and 2 and bare fraction for this case are given by,

$$\tilde{f}_1 = \left(\frac{c_1}{c_1 + m_1}\right) \quad (7)$$

$$\tilde{f}_2 = \frac{c_2(1-\tilde{f}_1)}{(c_1+c_2+m_2)} = \left(\frac{c_2 m_1}{(c_1+m_1)(c_1+c_2+m_2)}\right) \quad (8)$$

$$\tilde{f}_B = \frac{(m_1\tilde{f}_1+m_2\tilde{f}_2)}{(c_1+c_2)} \quad (9)$$

Unlike the classical version of the LV equations, the modified version of the equations does not require a minimum seeding fraction. In this case a PFT has the potential to expand as long as the climate is favorable and $c_i$ is positive. Finally, in equations (7) and (8) as long as $m_1 > 0$ and $c_2 > 0$ then PFT 2 will be able to exist and equilibrium coexistence is possible. Intermediate values of β give equilibrium values of fractional coverages of PFTs that lie in between those obtained by using β = 0 and β = 1. Melton and Arora (2016) discuss in detail why the use of β = 0 is more appropriate when simulating competition between PFTs, in contrast to simulating predator -prey interactions which traditionally uses β = 1.

In CTEM, the superiority or ranking of its seven natural non-crop PFTs is first based on the tree-grass distinction, where trees are considered to be always dominant over grasses because of their ability to shade them (Siemann and Rogers, 2003). Second, within the tree and grass PFTs the dominance is determined dynamically based on the colonization rate. The colonization rate of PFT α ($c_\alpha$, day$^{-1}$) is based on its net primary productivity ($NPP_\alpha$) and calculated as

$$c_\alpha = \zeta_\alpha \, \Lambda_\alpha \, max\,(NPP_\alpha, 0) \quad (10)$$

where $\zeta_\alpha$ is the inverse seedling density (m$^2$ (kg C)$^{-1}$) and $\Lambda_\alpha$ is the fraction of positive NPP (kg C m$^{-2}$ day$^{-1}$) allocated for expansion calculated based on the LAI (m$^2$ leaf /m$^2$ ground) of the PFT. The formulation of $\Lambda_\alpha$ is similar to that in Arora and Boer (2006) but with some differences.

$$\Lambda_\alpha = min\,(\lambda_{max}, max(\lambda_1, \lambda_2)) \quad (11)$$

where $\lambda_1$ and $\lambda_2$ are given by

$$\lambda_1 = \begin{cases} 0 & if\ LAI_\alpha \le LAI_{min} \\ \left(\frac{LAI_\alpha - LAI_{min}}{LAI_{max} - LAI_{min}}\lambda_{max}\right) & if\ LAI_{min} < LAI_\alpha < LAI_{max} \\ 1 & if\ LAI_\alpha \ge LAI_{max} \end{cases} \quad (12)$$

$$\lambda_2 = \begin{cases} \cosh\left(0.115(LAI_\alpha - 0.25LAI_{min})\right) - 1 & if\ LAI_\alpha > 0.25LAI_{min} \\ 0 & if\ LAI_\alpha \le 0.25LAI_{min} \end{cases} \quad (13)$$

where $LAI_\alpha$ is the LAI of PFT α. $LAI_{min}$ and $LAI_{max}$ are PFT-dependent parameters. $LAI_{max}$ is the upper threshold above which a maximum specified fraction of NPP ($\lambda_{max} = 0.1$) is used for expansion. The introduction of $\lambda_2$ term is new in version 2.0 of CTEM and ensures that a small fraction of NPP is allocated to expansion even at low LAIs. This change in the model parameterization yields better coverage of grasses.

The mortality rate ($m_\alpha$) represents the net effect of four different processes: a) intrinsic or age-related mortality ($m_a$), b) growth or stress mortality ($m_g$), c) mortality due to disturbance ($m_d$), and d) mortality due to adverse climate ($m_b$) and are calculated following Arora and Boer (2006).

$$m_\alpha = m_a + m_g + m_b + m_d \quad (14)$$

The components of equation (14) are described in more detail in Melton and Arora (2016). Briefly, the intrinsic mortality is calculated based upon PFT-specific maximum age and accounts for processes such as mortality caused by frost, hail and wind throw whose effects are not explicitly parameterized in the model. The growth mortality is dependent upon growth efficiency (biomass accumulated per unit leaf area) of a PFT over the last one year and initiated when a PFT doesn't do well as indicated by its growth efficiency. The mortality related to adverse climate that is parameterized in the model associated with long-term unfavourable climate and ensures that PFTs do not venture outside their bioclimatic zones. Finally, the mortality due to disturbance in the model is caused by fire which is parametrized using an intermediate complexity approach following Arora and Boer (2005a) with some additional changes as described in the context of version 2.0 of CTEM by Melton and Arora (2016). Briefly, the probability of fire is calculated using all three aspects of the fire triangle – fuel, moisture and ignition – represented by available above-ground biomass, soil moisture and natural (lightning) and anthropogenic ignition. Once known, the probability of fire is used to calculate area burned and the associated fire related $CO_2$ emissions. Fire reduces the standing vegetation biomass through $CO_2$ emissions directly to the atmosphere and through plant mortality but also creates bare ground which is subsequently available for colonization. The creation of bare ground depends on the susceptibility of each PFT to stand replacing fire (see equation A87 in Melton and Arora (2016)).

Finally, the fraction of grid cell covered by crops is not available for colonization, and neither does it gets burned. Consequently non-crop PFTs compete for space over the remaining fraction of the grid cell.

## 3. Experimental set up and methodology

The CLASS-CTEM model was configured in the composite and mosaic modes to simulate competition at selected seven sites that represent a variety of climatic conditions including sites in the Amazonian region (tropical forests), India (sub-tropical forests), South Sudan (savanna ecosystems), California and Vancouver Island (temperate forests), Siberia (boreal forests), and the Tibetan Plateau (grasslands), as shown in Figure 1.

The CLASS-CTEM model is driven with CRU-NCEP climate data (surface temperature, pressure, precipitation, wind, specific humidity, shortwave and longwave radiation fluxes) which are available at a resolution of 0.5 degrees and at a six hourly time interval (http://dods.extra.cea.fr/data/p529viov/cruncep). The CRU-NCEP data are based on the National Centre for Environmental Prediction (NCEP) reanalysis (Kanamitsu et al., 2002) but its monthly mean values are adjusted to match data from the Climate Research Unit (CRU) observations. These data were interpolated to the 96 × 48 Gaussian spatial resolution which corresponds to ~3.75º. In the Canadian earth system modelling framework, the CLASS and CTEM models are applied at large spatial scales and hence the decision to choose this resolution. The 6-hourly CRU-NCEP climate data were interpolated to a half-hourly time resolution following the approach of Arora and Boer (2005a). Temperature, long-wave radiation, wind speed, specific humidity, and pressure were linearly interpolated in time; short-wave radiation was assumed to change with solar zenith angle with a maximum value at the local solar noon; precipitation was disaggregated using the six-hourly precipitation amount to estimate the number of wet half hours, and total 6-hourly precipitation amount is randomly but conservatively distributed over the wet half hours. Regardless of the representation of sub-grid scale variability of vegetation (composite or mosaic), all PFTs are driven with the same meteorological data and respond to the same soil texture within a grid

cell.

The model simulations are initialized with zero biomass and zero fractional coverage for all non-crop PFTs. The fractions of $C_3$ and $C_4$ crop PFTs are prescribed based on the reconstruction of historical land cover following Wang et al. (2006), as explained below. Atmospheric $CO_2$ concentration is set to 350 ppm, as opposed to current value of around 400 ppm since the current state of vegetation is not in equilibrium with atmospheric $CO_2$. The simulations are run for 400 years, driven by 1901-1940 meteorological forcing data used repeatedly. Climate data are used from the 1901-1940 period, as opposed to those from the later part of the 20$^{th}$ century, because these data do not show a warming trend (Wen et al., 2011). In addition, the simulated fractional coverage of PFTs are more sensitive to change in $CO_2$ concentration than to change in climate (e.g. the 1901-1940 period compared to that for the present day). The 400 year timescale is sufficient for simulated fractional coverage of all PFTs to reach equilibrium at all locations.

We use observation-based estimates of fractional coverage of PFTs based on (Wang et al., 2006) (hereafter WANG06) and the Moderate Resolution Imaging Spectroradiometer land cover product (Friedl et al., 2013) (hereafter MODIS) to evaluate the fractional coverage of the seven non-crop PFTs simulated by CTEM. WANG06 (their Table 2) mapped 22 land cover types of the Global Land Cover for the year 2000 (GLC2000) to the nine PFTs represented in CTEM listed in Table 1. They then reconstructed land cover back in time to 1850 by taking into account changing crop area using the Ramankutty and Foley (1999) crop area data set. Here, instead we have used the newer HYDE v. 3.1 crop data set (Hurtt et al., 2011) which yields land cover for the 1850-2012 period at 0.5° resolution and we refer to this reconstructed historical land cover as the modified WANG06 product. The MODIS land

cover product is available at 0.5° resolution and contains 17 land cover types which are mapped to the nine PFTs represented in CTEM in a manner similar to Table 2 of WANG06. The MODIS data are available for the period 2001 – 2011 and their average over this period was used. Finally, both the modified WANG06 and MODIS products are interpolated to the 3.75° grid resolution, similar to the resolution of the climate data.

The interpretation of simulated fractional coverage of PFTs based on comparison to these observation-based data products is susceptible to at least two errors. First, the categorization of the remotely-sensed vegetation to the 22 vegetation types in the GLC2000 dataset and the 17 vegetation types in the MODIS product is subject to error. This categorization is based on vegetation reflectance in the visible and infrared bands (e.g. see Figure 1 of (Latifovic et al., 2004)) and ground truthing. Second mapping of those vegetation types to the nine PFTs represented in CTEM introduces further error. Land cover classification is inherently a subjective process, so the uncertainty in classification can never be totally accounted for. As a result, the comparison of simulated fractional coverage of PFTs to observation-based estimates at the most basic tree-grass-bare level is expected to be more robust than the comparison at the level of individual PFTs. Nevertheless, we have more confidence in the WANG06 product because it was designed specifically to map 22 vegetation types in the GLC2000 land cover product to CTEM's nine PFTs.

The difference in modelled values of the coverage of seven non-crop CTEM's PFTs ($f_{m,i}$) compared to the modified WANG06 product ($f_{o,i}$) is represented in terms of the root mean square error (RMSE) for both the composite and mosaic configurations,

$$RMSE = \sqrt{\frac{\sum_{i=1}^{7}(f_{o,i} - f_{m,i})^2}{7}}. \quad (15)$$

Root mean square difference (RMSD) is used to compare using the simulated equilibrium coverage of the seven non-crop PFTs from the composite ($f_{m\_c,i}$) and mosaic ($f_{m\_m,i}$) approaches

$$RMSD = \sqrt{\frac{\sum_{i=1}^{7}(f_{m\_c,i} - f_{m\_m,i})^2}{7}}. \quad (16)$$

The calculated RMSE, for the composite and mosaic approaches, allows to compare simulated coverages to observation-based estimates from WANG06, and RMSD allows to compare the two approaches to each other.

Simulated fractional coverage of individual PFTs at equilibrium are compared with observation-based estimates based on the modified WANG06 product, and at the basic tree-grass-bare level with observation-based estimates from both the modified WANG06 and MODIS products. The MODIS product is not used for comparison at the individual PFT level because our methodology to map 17 land cover types in the MODIS product to the nine PFTs represented in CTEM is not ground truthed as the WANG06 approach has been.

Finally, a heterogeneity index (*H*) is calculated following Melton and Arora (2014) (their equation 4) which characterizes land cover heterogeneity as

$$H = 1 - \frac{\frac{1}{N-1}\sum(f_i - \overline{f})^2}{\overline{f}} \quad (17)$$

where $f_i$ is the fractional coverage of CTEM's PFTs at equilibrium, $\overline{f}$ their mean and *N*=9 (including the seven non-crop and two crop PFTs as shown in Table 1). Regions of high PFT heterogeneity (grid cells with many different PFTs) have *H* index values close to 1 while regions of low PFT heterogeneity (grid cells with few PFTs present) are close to 0. Equation

(17) yields an *H* value of 1 if a grid cell contains N PFTs and the bare fraction each occupying $\left(\frac{1}{N+1}\right)^{th}$ fraction of the grid cell, indicating maximum possible heterogeneity, and a value of 0 if an entire grid cell is occupied with only a single PFT.

## 4. Results and discussion

Results from model simulations, based on the modified version of the LV equations used in version 2 of CTEM, at the seven selected sites are shown in Figure 2 through 8. These figures show the evolution of the simulated fractional coverage of PFTs when starting from bare ground, snapshots of fractional coverages of PFTs for two selected years and compare simulated fractional coverages of PFTs to observation-based estimates.

### 4.1 Tropical region

#### a. Amazonia

In the Amazonia, observed forest recovery in cut, burnt and abandoned forests shows an emergence of herbaceous plants after fire, which attain maximum coverage within three to four years and decline thereafter, subsequently taken over by tree species after eight years of establishment (Uhl et al., 1988). CLASS-CTEM is successfully able to reproduce this successional behaviour. Figure 2a and 2b show the evolution of simulated fractional coverages of PFTs for composite and mosaic configurations of the model. $C_3$ and $C_4$ grasses dominate initially, with $C_4$ grasses covering a larger fraction because of their higher productivity compared to $C_3$ grasses (Williams et al., 2013), and achieve their maximum coverage within three to four years, followed by a rapid decline in grass cover. Broadleaf evergreen (BDL EVG) trees outcompete grasses after about six years, slightly earlier than observations. Equilibrium coverage is attained after about 50 years. This evolution pattern is similar in both the composite and mosaic configurations of the model. The rapid expansion of

grasses and thereafter that of BDL EVG trees, and the overall large fraction of the grid cell being covered with trees, are consistent with warm and wet climatic conditions at this location. Mean annual precipitation and temperature, based on the CRU-NCEP climate data, at this location are 2110 mm and 26.9 °C, respectively.

Figures 2c and 2d show the snapshot of simulated fractional coverages of model PFTs at years 5 and 50 for the composite and mosaic configurations respectively, which reveal an identical composition of PFTs at this location in both configurations. Comparison with the modified WANG06 product for individual PFTs indicates (Figure 2e) that the model is able to reproduce realistic coverage of broadleaf evergreen trees, and $C_3$ and $C_4$ grass PFTs at this location, with the caveat that both observation-based estimates suggest near full coverage by the tree PFT while the model simulates a small amount of grasses (Figure 2f) and bare fraction. At equilibrium, grasses cover around 1-3% of the grid cell while 93% of the grid cell is covered by BDL EVG trees in both configurations, which is somewhat less than the observation-based estimate of around 100 % coverage. Both the original and modified versions of the LV equations are limited in that neither can yield a 100% coverage of a PFT in a grid cell as long as the mortality term ($m$) is greater than zero (see equations 4 and 7).

The RMSE is similar between the composite (2.3%) and mosaic (2.5%) approaches when modelled results are compared to observation-based estimates from the modified WANG06 product (see Table 2) and so are the successional patterns in Figure 2a and 2b. This is expected because when a grid cell is dominated by a single PFT, and characterized by a low heterogeneity index, then both the composite and mosaic configurations yield similar results. Melton and Arora (2014) show that differences between the composite and mosaic configurations are largest in grid cells where more PFTs exist and heterogeneity index is

higher. With only three PFTs that can exist in this Amazonian grid cell, and only one being dominant, surface heterogeneity is low ($H$ = 0.11 and 0.12 in composite and mosaic configurations, respectively) and as a consequence composite and mosaic configurations yield similar results.

### 4.2 Subtropical region

#### a. India

The grid cell in India has extensive $C_3$ and $C_4$ crops whose fractional coverages are specified based on the modified WANG06 product. Combined $C_3$ and $C_4$ crops cover 42% of the grid cell. Competition between PFTs then determines their coverage over the remaining 58% of the grid cell. The model correctly simulates the existence of the BDL EVG and broadleaf dry deciduous (BDL DCD DRY) trees, and $C_3$ and $C_4$ grasses (Figure 3e). $C_3$ and $C_4$ grasses dominate initially and achieve their maximum coverage in the first 4 – 10 years (Figure 3a and 3b). The fractional coverage of both grasses decrease thereafter as trees slowly increase their areal extent. Evolution of the fractional coverages of PFTs and their equilibrium values are somewhat different in the composite and mosaic configurations. Near equilibrium values of fractional coverage of PFTs are obtained after about 60 years in both configurations. Both BDL EVG and BDL DCD DRY trees increase their expanse at a somewhat faster rate in the mosaic configuration and eventually also equilibrate at higher values of their fractional coverages, although the difference is more pronounced for BDL DCD DRY trees. At near equilibrium the coverage of BDL DCD DRY trees is higher in the mosaic (28%) than in the composite configuration (17%). $C_3$ and $C_4$ grasses, in contrast, equilibrate at lower values of fractional coverage in the mosaic configuration. The combined coverage of $C_3$ and $C_4$ grasses is 13% in the mosaic compared to 24% in the composite configuration. The reason for higher (lower) coverage of trees (grasses) in the mosaic configuration is related to the manner in

which the representation of sub-grid scale variability of vegetation affects surface albedo and consequently net shortwave radiation, as discussed in Li and Arora (2012). Since trees are darker than grasses they are characterized by lower values of surface albedos than grasses in the model. In the composite configuration, an average surface albedo value is used that is based on albedo of the individual PFTs weighted by their fractional coverage. In the mosaic configuration each PFT's albedo is used to calculate the net radiation it receives. As a result, trees (grasses) receive more (less) radiation in the mosaic compared the composite configuration. Other state variables respond to these changes in net radiation, so soil moisture and temperature evolve differently in the two configurations and in some cases their effect can overcome the effect of the differences in net radiation (Li and Arora, 2012). At this location in India, however, the first order effect of net radiation dominates.

Mean annual precipitation (1074 mm) at this location in India is much lower than that in Amazonia (2110 mm) although the mean annual temperature is similar (26.5 °C). As expected then, the rate of spread of grasses and trees is slower and at near equilibrium trees cover a much lower fraction of the grid cell than is available for colonization. Compared to 93% tree coverage in Amazonia for both the composite and mosaic configurations, here the trees cover 24% and 36% of the grid cell out of available 58% (since 42% is covered by crops) or equivalently 42% and 62% of the available area in the composite and mosaic configurations, respectively. These differences are also seen in the snapshots of simulated fractional coverages of model PFTs at years 5 and 60, in Figures 3c and 3d.

In Figure 3e, compared to reconstructed historical land cover based on the modified WANG06 product, the CLASS-CTEM model overestimates BDL EVG trees by ~5% (~4%) and underestimates BDL DCD DRY trees by 18% (29%) in the mosaic (composite)

configuration. Consequently, based on this comparison, the model overestimates $C_3$ and $C_4$ grasses by ~6% (~12%) and ~5% (~10%) in the mosaic (composite) configuration. However, the comparison at the basic tree-grass-bare level in Figure 3f indicates that the simulated tree, grass and bare fractions lie in between the modified WANG06 and MODIS estimates. In Figure 3e, the mosaic configuration yields a somewhat better comparison with the modified WANG06 product as also seen in the RMSE values for mosaic (RMSE = 7.6%) and composite (RMSE = 12.5%) configurations in Table 2. The heterogeneity index is high for this location ($H$ = 0.92 and 0.89 in composite and mosaic configurations, respectively) since six different PFTs and some bare ground fraction exist.

### 4.3 Savanna

#### a. South Sudan

The South Sudan site is characterized by 8% crop area, of which 1% is covered by $C_3$ crops and 7% by $C_4$ crops, so the remaining fraction of 92% is available for colonization by non-crop PFTs. Mean annual precipitation at this location is 822 mm and the average annual temperature is around 27 °C.

CLASS-CTEM simulates a mix of BDL EVG and BDL DCD DRY trees and $C_3$ and $C_4$ grasses at this savanna site in South Sudan (Figure 4a and 4b). Bare ground is rapidly colonized by $C_3$ and $C_4$ grasses initially, with $C_4$ grasses attaining their maximum coverage (~60%) after about three years and $C_3$ grasses achieve their maximum extent (~45%) in about eight years. The model allows $C_3$ and $C_4$ grasses to co-exist at equilibrium but their coverages show an out-of-phase oscillatory behaviour with a timescale of about 10-12 years. This time scale is roughly consistent with the fire return interval at this location. The oscillatory behaviour of the fractional coverages of $C_3$ and $C_4$ grasses disappears when simulations are

carried out without fire (not shown). In simulations without fire the coverage of BDL DCD DRY trees is higher as would be expected since disturbance due to fire allows grasses to better coexist with trees. $C_3$ and $C_4$ coexist in the simulations without fire, albeit with a higher fractional coverage of $C_3$ grasses. When disturbance due to fire is present, $C_4$ grasses are able to colonize the available bare fraction faster after a disturbance because of their higher productivity. Gradually $C_3$ grasses also begin to recover and compete with $C_4$ grasses for space up until the next fire event after which $C_4$ grasses get the opportunistic advantage again to colonize at a faster rate. The oscillatory behaviour of fractional coverage of $C_3$ and $C_4$ grasses in Figure 4 is caused by this phenomenon but also the 40-year 1901-1940 climate that is repeatedly used to drive the CLASS-CTEM model. For example, fire events that occur in a given 40-year cycle associated with specific climatic conditions return in the next cycle when the same climatic conditions return again. Although the role of fire in expansion of $C_4$ grasses is not completely understood these results are broadly consistent with those of (Scheiter et al., 2012) (and references therein) who suggest that the more flammable foliage, higher allocation to below ground  roots and rapid regrowth after fire that characterize $C_4$ grasses help them increase their expanse in the presence of fire. The fire module of CTEM (see section A9 in Melton and Arora, 2016) does not distinguish between flammability of $C_3$ and $C_4$ grasses, so only the rapid regrowth of $C_4$ grasses after fire contributes to their increased fractional coverage in the CLASS-CTEM modelling framework.

In Figure 4, BDL EVG and BDL DCD DRY trees start to increase their expanse after about 10 years and equilibrium is attained after about 80 years. At equilibrium, the grass PFTs occupy a larger fraction of the grid cell in the composite approach, compared to the mosaic approach, whereas the opposite is true for the tree PFTs. This is attributed to higher net shortwave radiation available for grass PFTs and lower net shortwave radiation for tree PFTs

in the composite compared to the mosaic configuration, as mentioned earlier. In addition, the difference between the composite and mosaic configurations is more pronounced than the site in India, especially for BDL DCD DRY trees. The combined coverage of $C_3$ and $C_4$ grasses is 37% in the composite and 15% in the mosaic configuration. The combined coverage of trees is 39% in the composite configuration and 62% in the mosaic configuration, as seen in Figures 4c and 4d. Since only 92% of the grid cell is available for colonization by non-crop PFTs, the coverage of trees of 39% and 62%, in the composite and mosaic configurations, corresponds to 42% and 66% of the available area for colonization. This is similar to the location in India given that both locations experience similar climate. The differences in the successional behaviour of PFTs, as their fractional coverages evolve over time, in the composite and mosaic configurations are seen in the snapshots of fractional coverage of PFTs at year 13 and 95 in Figure 4c and 4d, and consistent with the higher heterogeneity index at this location ($H$ = 0.87 and 0.71 in the composite and mosaic configurations, respectively).

The comparison of simulated fractional coverage of nine PFTs with the observation-based estimate from the modified WANG06 data set (in Figure 4e) shows that the model successfully simulates the existence of correct PFTs at this location (Figure 4c). Compared to the modified WANG06 data set, however, the coverage of BDL DCD DRY trees is overestimated by ~26% (~5%) and underestimated for grasses PFTs by ~27% (~5%) in the mosaic (composite) approach. As expected then, the RMSE values confirm that the composite configuration (RMSE = 10.3%) performs better than the mosaic configuration (RMSE = 16.2%) (Table 2) at this location. In addition, while the model simulates nearly equal fractions of $C_3$ and $C_4$ grasses, the modified WANG06 data set suggests that $C_4$ grasses are dominant at this location. The $C_3$ and $C_4$ fractions of crop and grass fractions in each grid cell in the WANG06 data set are based on the global distribution of $C_4$ vegetation developed by

Still et al. (2003), which is a part-observation and part-model based product. Comparison of modelled fractional coverages at the basic tree-grass-bare level (Figure 4f) with modified WANG06 and the MODIS-based products shows that the model reproduces realistic fractions of vegetated and bare land fractions.

For a tropical savanna location in Botswana, Heinl et al. (2007) find that herbaceous plants achieve their maximum coverage within 4 to 8 years after fire. Their coverage reduces thereafter due to competition with woody plants which become dominant after about 12 years. While CLASS-CTEM largely reproduces this pattern of successional dynamics, the BDL DCD DRY trees take about 20 years to become the dominant PFT in the mosaic configuration and about 40 years in the composite configuration. One possible reason for the slow rate of expansion for trees in the model is that in the real world drought deciduous trees that are affected by fire have adaptive mechanisms (e.g. shoots sprout from existing burnt or fallen trees) to deal with post-fire conditions (Omi, 2005). Sprouts grow much faster than seedlings and are able to quickly reoccupy gaps. In contrast, in the model the trees are assumed to grow from seedlings (parameterized through seedling density in equation 10) that get established on the bare ground.

### 4.4 Temperate region

#### a. California

The temperate site in California experiences a much cooler and drier climate than the sites considered so far. Mean annual temperature at this location is 13.4 °C and mean annual precipitation only 422 mm, based on the CRU-NCEP climate data. The $C_3$ crops cover 9% of the grid cell and competition therefore determines the coverages of PFTs over the remaining 91% of the grid cell.

CLASS-CTEM simulates a mixture of $C_3$ grasses and needleleaf evergreen (NDL EVG) trees at this temperate location (Figure 5a and 5b). The $C_3$ grasses initially dominate and attain maximum coverage (~70%) within the first 5 years, which is consistent with observed post-fire recovery in shrublands of southern California where herbaceous plants cover 80% area of land (Keeley et al., 1981) in 3-5 years after fire and reduce thereafter (Keeley et al., 2005). The fractional coverage of $C_3$ grasses declines as NDL EVG trees slowly increase their expanse starting around year 25. The slow and late increase in the expanse of NDL EVG trees is consistent with cooler and drier climatic conditions (Bonan and Sirois, 1992). The model successfully simulates a small fraction (2-3%) of the grid cell covered by BDL EVG trees, consistent with the modified WANG06 product. The model is also able to simulate NDL EVG trees as the dominant woody PFT consistent with observations that NDL EVG trees perform well in regions where maximum precipitation and temperature are out of phase with each other (Stephenson, 1998) as is the case on the western Pacific coast of the United States and Canada. The summer growing season with less rainfall implies that evergreen conifers outcompete deciduous trees because of their low transpiration rates in summer as well as their ability to take advantage of the moisture available during the wet mild winter months when they still have their leaves on. Equilibrium is attained for the NDL EVG trees about 100-150 years sooner in the mosaic configuration compared to the composite configuration. At equilibrium, NDL EVG trees cover 11% more and $C_3$ grasses cover 12% less area of the grid cell in mosaic compared to the composite configuration. Both these aspects are consistent with trees receiving higher net shortwave radiation in the mosaic configuration, although the differences in time to equilibrium for tree PFTs were hardly noticeable for locations considered earlier. Figures 5c and 5d, which show the snapshots of fractional coverages at years 20 and 300 show the differences between the composite and mosaic configurations.

The comparison of simulated fractional coverage of CTEM's non-crop PFTs with observation-based estimates from the modified WANG06 data set is shown in Figure 5e. The simulated fractional coverage of NDL EVG trees is overestimated because the model does not simulate any fractional cover for broadleaf cold deciduous (BDL DCD CLD) trees, while the modified WANG06 data sets suggests coverage of about 18%. One possible reason for the model to not simulate any fraction of the grid cell covered by BDL DCD CLD trees is the coarse resolution of the model and the driving climate data. At the resolution of 3.75 degrees (around 350 kilometers) it is reasonable to assume that the use of average climate cannot capture climate niches that occur given the variations in local topography. This is particularly important at this location which is characterized by large variations in topography and the resulting diversity in climate varying from mild conditions near the coastal regions and colder conditions at higher elevations (Kauffman, 2003). At the basic tree-grass-bare level, the simulated fractional coverages compare reasonably to the estimates based on modified WANG06 and the MODIS-based products. When comparing simulated fractional coverages for all the nine PFTs to the modified WANG06 data, the RMSE analysis shows that the composite configuration (RMSE = 10.2%) performs better than the mosaic configuration (RMSE = 13.5%) at this location (Table 2). The relatively large RMSD (6.2%) indicating differences between simulated fractional coverage of PFTs in the composite and mosaic configurations is also consistent with high heterogeneity at this location ($H$ = 0.72 and 0.62 for the composite and mosaic configurations, respectively).

**b. Vancouver Island**

The temperate site on Vancouver Island, on the western coast of Canada, experiences wet and cool winters and dry and warm summers. The mean annual precipitation at this location is

1101 mm, of which about 70 % falls from October through March, and the mean annual temperature is 3.6 °C.

Given the dry and warm summers, and the wet and cool winters, the location is ideally suited for NDL EVG trees which take advantage of their low transpiration rates and their ability to retain leaves year round, as mentioned earlier. Consistent with the modified WANG06 product, CLASS-CTEM simulates coniferous forest at this location (Figure 6e). $C_3$ grasses dominate initially, and achieve more than 70% coverage by year 25 and then decline thereafter as the slow growing NDL EVG trees gradually increase their expanse (Figures 6a and 6b). This may be compared with establishment period of ~20 years after fire for black and white spruce in the southeast of Yukon region (Johnstone et al., 2004). BDL DCD CLD trees are able to survive briefly covering a small fraction of the grid cell but are unable to outcompete NDL-EVG trees, given the dry summers which is the only time during which BDL DCD CLD trees have their leaves on. This successional pattern is similar for both the composite and mosaic configurations although some differences exist. During the first 100 years of the simulation, $C_3$ grasses cover a larger fraction of the grid cell in the composite than in the mosaic configuration primarily because grasses receive more net shortwave radiation in the composite configuration, as also seen in Figures 6c and 6d which show the snapshot of fractional coverages of PFTs at years 27 and 190. This pattern of grasses performing better in the composite compared to the mosaic configuration is also seen at locations in India, Sudan and California.

In Figure 6e, the model correctly simulates NDL EVG trees as the dominat PFT. However, compared to the modified WANG06 product (~70% coverage), the coverage of NDL-EVG trees is overestimated by about 10% in both composite and mosaic configurations (~80%

coverage). At equilibrium, BDL EVG trees are excluded in both the composite and mosaic configurations and BDL DCD CLD trees are excluded in the composite configuration. The fractions of these PFTs are, however, small based on the modified WANG06 data set. The RMSE values shows that the mosaic configuration yields slightly better results (RMSE = 5.6%) than the composite (RMSE = 6.5%) configuration. When comparing the fractional coverages at the basic tree-grass-bare level, the model results also compare well with the observation-based estimates based on the modified WANG06 and MODIS products. (Figure 6f). The small RMSD value of 0.8% indicates that the simulated fractional coverage of PFTs in the composite and mosaic configurations are very similar which is consistent with low heterogeneity at this location ($H$ = 0.24 and 0.20 for the composite and mosaic configurations, respectively).

### 4.5 Boreal region

#### a. Siberia

The mean annual precipitation and the mean annual temperature at the location in Siberia are 481 mm and −1.9 °C, respectively. This boreal forest location in northwest Siberia is characterized by mixed forests consisting of NDL EVG and BDL DCD CLD trees and $C_3$ grasses (Figure 7e). CLASS-CTEM is successfully able to simulate this mix of PFTs. $C_3$ grasses dominate initially and achieve maximum coverage (~70%) after about 10 years. This is broadly consistent with an experimental study in the western Siberian plains, where eight years after a stand replacing fire herbaceous plants and mosses covered ~75% of the area (Kovaleva and Ivanova, 2013). Thereafter, the coverage of grasses declines gradually as the NDL EVG and BDL DCD CLD trees increase their expanse. While the fractional coverage of relatively fast growing BDL DCD CLD trees reaches near equilibrium around year 80, the

fractional coverage of slow growing NDL EVG trees reaches equilibrium much later (Figures 7a, 7b). In fact, in the mosaic configuration the fractional coverage of NDL EVG trees keep slowly increases even at year 200. This is an expected behaviour given the cold temperatures (Bonan and Sirois, 1992) and low solar radiation at this high- latitude location. The evolution of fractional coverages of PFTs is similar in the composite and mosaic configurations as also seen in the snapshots of fractional coverages of PFTs at years 9 and 190 in Figures 7c and 7d. This composition is consistent with observed plant community in this area. Blyakharchuk et al. (2007) report broadleaf cold deciduous Birch trees and needleleaf evergreen Scots Pine trees as the principal trees species along with herbaceous plants in this area.

At equilibrium, the simulated coverages of PFT are broadly similar in both the composite and mosaic configurations. The model is, however, unable to simulate the NDL EVG trees as the dominant tree PFT at this location as the observation-based modified WANG06 product suggests; the model simulates BDL DCD COLD trees as the dominant PFT (Figure 7). The RMSE values shows that the composite configuration yields slightly better results (RMSE = 18.4%) than the mosaic (RMSE = 20.2%) configuration. The overall tree, grass and bare fractions in Figure 7f, however, compare reasonably with the modified WANG06 and MODIS based products. The RMSD value of 2.2% indicates that the simulated fractional coverage of PFTs in the composite and mosaic configurations are similar although this location is characterized by relative high heterogeneity ($H$ = 0.70 and 0.66 for the composite and mosaic configurations, respectively).

### 4.6 Grassland

#### a. The Tibetan Steppe

The last location at which the performance of CTEM's competition parameterization is evaluated is the Tibetan grasslands. These grasslands are one of the largest grazing ecosystems in the world and characterized by arid to semi-arid climate (Miller, 2005). The grid cell chosen in this region receives an annual rainfall of 435 mm and the average temperature remains below freezing level at –3.35 °C. Miller (1995) report that vegetation in the Tibetan Plateau region is primarily composed of grasses that cover about 70% of the area. This estimate is broadly consistent with the modified WANG06 dataset (~60%) shown in Figure 8f. The absence of trees at this location is due to low annual precipitation and cold temperatures, although the MODIS-based product suggests a small fractional coverage for trees.

Consistent with the observation-based estimates the only model PFT that can grow at this location is $C_3$ grasses. $C_4$ grasses, which are poor competitors to $C_3$ grasses in colder climate (Baskin and Baskin, 1978) (Yamori et al., 2013;Stensrud, 2009), are outcompeted. The model tree PFTs are excluded at this location due to bioclimatic constraints. In the absence of competition from trees the $C_3$ grasses are able to colonize a relatively large fraction of the grid cell. The composite and mosaic configurations both yield similar evolution of $C_3$ grasses (Figure 8a-8d) and maximum coverage is reached around year 20 because of the cold and dry climate and the consequential slow rate of expansion. $C_3$ grasses cover about 66% and 64% of the grid cell, respectively, in the composite and mosaic configurations at equilibrium consistent with the observation-based modified WANG06 data set and the estimate from Miller (2005) (Figure 8c-8d). The RMSE error for both the mosaic and composite configurations is also similar (~9%), and the RMSD is low consistent with low heterogeneity

($H$ = 0.34 and 0.37 in the composite and mosaic configurations, respectively).

## 5. Summary and conclusions

This study evaluates the competition parameterization of the CLASS-CTEM model at selected locations across the globe. Our objective was to assess if the model is successfully able to reproduce the observed mix of PFTs and their fractional coverages and to what extent the simulated competition between PFTs is affected by the manner in which the sub-grid scale variability of vegetation is represented (i.e. the use of the composite versus the mosaic configuration). Our study also aimed to assess the simulated successional dynamics of vegetation against available empirical evidence.

The results show that the model is able to reproduce broad scale successional patterns of vegetation dynamics. When starting from a bare ground state, all the study sites show an initial high abundance of herbaceous plants that is attained within a few years, followed by dominance of trees as long as the climate is favorable. In addition, the time to achieve equilibrium for fractional coverage of trees is shorter when climate is more favourable (e.g. 30-40 years at the Amazonian site) compared to harsher climates (e.g. 100-150 years at the Siberia site). These broad scale successional patterns are expected and are realistic as empirical evidence suggests, although difference exists in simulated values and information available from empirical evidence.

Root mean square difference (RMSD), which quantifies the difference between the composite and mosaic configurations of the model, is smaller than RMSE at all sites, implying that the modelled results from the composite and mosaic configurations are closer to each other than to observation-based estimates of fractional coverage of PFTs based on the modified

WANG06 data set. These results suggest that the simulated fractional coverages of PFTs are not overly sensitive to representation of sub-grid scale variability of vegetation. The composite and mosaic configurations, however, do yield different results especially at the sub-tropical/savanna locations of India and South Sudan, but also at the location in California. The heterogeneity index is also high at these locations. Intuitively and based on results from Melton and Arora (2014) we expect the composite and mosaic configurations to yield different results when land cover heterogeneity is high. At these locations the fractional coverage of trees is higher in the mosaic than in the composite configuration because of higher net shortwave radiation they receive while the opposite is true for grasses. Simulated fractional coverages of PFTs are more similar between the composite and mosaic configurations at locations which are characterized by low vegetation heterogeneity; these include the site in the Amazonian region, on Vancouver Island in Canada and the grassland location in the Tibetan Plateau region.

When comparing simulated fractional coverage of PFTs to observation-based estimates, the model is most successful at the basic tree-grass-bare ground level. The observation-based estimates at the most basic tree-grass-bare level are also expected to be more robust than the observation-based fractional coverage of individual PFTs. The latter require assumptions when mapping land cover types from typical land cover products to the individual PFTs that are represented in models (e.g. see Table 2 of Wang et al., 2006). When compared to observation-based estimates of the modified WANG06 data set for the individual PFTs, the model does a reasonable job at most locations considered but some limitations remain. At the California location, the model fails to capture the existence of broadleaf cold deciduous trees (Figure 5). At the Siberia location the model simulates broadleaf cold deciduous trees as the dominant PFT but observation-based estimate suggests that needleleaf evergreen trees are the

dominant PFT here and about 20% of the grid cell here is covered by broadleaf evergreen trees (Figure 7). The latter is incorrectly classified in the WANG06 product who categorize high-latitude evergreen shrubs as broadleaf evergreen trees, while in CTEM broadleaf evergreen trees are limited only to tropical regions.

The limitations of the model to correctly simulate fractional coverages at the individual PFT level are in part due to difficult comparison with observation-based estimates but also the limited number of natural PFTs (seven) that are represented in the model and the coarse resolution (3.75° ) at which the model is run. For example, CLASS and CTEM do not currently represent shrubs. At the large spatial resolution at which the model is implemented it is unable to represent PFTs that are able to exist in climate niches associated with large variations in topography.

The model is also able to simulate the coexistence of $C_3$ and $C_4$ grasses driven in part by disturbance due to fire consistent with empirical evidence. $C_4$ grasses are potentially able to dominate after a disturbance due to their higher water use efficiency (Black, 1973;Williams et al., 2013) and greater $CO_2$ assimilation capacity over $C_3$ plants (Black, 1971) which allows them to colonize faster. The higher productivity and water use efficiency of $C_4$ grasses are represented in the model.

Overall the CLASS-CTEM model simulates reasonably realistic fractional coverage of trees, grasses and bare land. The simulated successional dynamics including initial dominance by herbaceous PFTs followed by woody PFTs, climate permitting, are also simulated broadly consistent with available empirical data. The evaluation of CLASS-CTEM at the sites presented in this study suggest that the competition parameterization of the model behaves

realistically enough to be used as a tool to project changes in vegetation distribution associated with changes in climate and atmospheric $CO_2$ concentration. Finally, given the fairly similar simulated fractional coverages of PFTs when using the composite and mosaic configurations, the model results suggest the use of the composite approach given its low computational expense. Whether the similarity between the two configurations holds at the global scale can only be verified by performing global simulations and this work is planned as a future exercise.

*Author contribution.* V. A. and J. M. designed the experiment and provided feedbacks. R.S. ran simulations, created figures, performed analyses. R.S. and V.A. wrote the manuscript.

*Acknowledgements.* R. K. Shrestha was supported by Canadian Network for Regional Climate and Weather Processes (CNRCWP) that is funded by the Climate Change and Atmospheric Research initiative of National Scientific and Engineering Research Council of Canada (NSERC). The authors also thank the two anonymous reviewers for their constructive comments and suggestions. The model code and the data used to plot results in Figures 2 through 8 can be obtained from V. A. (vivek.arora@canada.ca).

**References**

Anand, M., 2000: The fundamentals of vegetation change - complexity rules. *Acta Biotheoretica*, **48**, 1-14.

Arora, V. K., 2003: Simulating energy and carbon fluxes over winter wheat using coupled land surface terrrestrial ecosystem models. *Agriculture and Forest Meteorology*, **118**, 21-47.

Arora, V. K., and G. J. Boer, 2003: A representation of variable root distribution in dynamic vegetation models. *Earth Interactions*, **7**, 1-19.

Arora, V. K., and G. J. Boer, 2005a: Fire as an interactive component of dynamic vegetation models. *J. Geophys. Res.*, **110**, G02008.

Arora, V. K., and G. J. Boer, 2005b: A parameterization of leaf phenology for the terrestrial ecosystem component of climate models. *Glob. Change Biol.*, **11**, 39-59.

Arora, V. K., and G. J. Boer, 2006: Simulating Competition and Coexistence between Plant Functional Types in a Dynamic Vegetation Model. *Earth Interactions*, **10**, 1-29.

Arora, V. K., J. F. Scinocca, G. J. Boer, J. R. Christian, K. L. Denman, G. M. Flato, V. V. Kharin, W. G. Lee, and W. J. Merryfield, 2011: Carbon emission limits required to satisfy future representative concentration pathways of greenhouse gases. *Geophys. Res. Lett.*, **38**, L05805.

Baskin, J. M., and C. C. Baskin, 1978: A discussion of the growth and competitive ability of C3 and C4 plants. *Castanea*, **43**, 71-76.

Begon, M., J. Harper, and C. R. Townsend, 1986: Ecology: Individuals, Populations and Communities, Blackwell Scientific Publications, Oxford 876 pp.

Berger, U., C. Piou, K. Schiffers, and V. Grimm, 2008: Composition among plants: Concepts,

individual-based modelling approaches, and a proposal for a future research strategy. *Perspectives in plant ecology, evolution and systematics*, **9**, 121-135.

Black, C. C., Jr., 1971: Ecological implications of dividing plants into groups with distinct photosynthetic production capacities *Adv. Ecol. Res.*, **7**, 87-114.

Black, C. C., Jr., 1973: Photosynthetic carbon fixtation in relation to net CO2 uptake. *Ann. Rev. Plant Physiol.* , **24**, 253-286.

Blyakharchuk, T. A., H. E. Wright, P. S. Borodavko, W. O. van der Knaap, and B. Ammann, 2007: Late Glacial and Holocene vegetation history of the Altai Mountains (southwestern Tuva Republic, Siberia). *Palaeogeography, Palaeoclimatology, Palaeoecology*, **245**, 518-534.

Bonan, G. B., and L. Sirois, 1992: Air temperature, tree growth, and the northern and southern range limits to *Picea mariana*. *J. Veg. Sci.*, **3**, 495-506.

Bond-Lamberty, B., S. D. Peckham, S. T. Gower, and B. E. Ewers, 2009: Effects of fire on regional evapotranspiration in the central Canadian boreal forest. *Global Change Biology*, **15**, 1242-1254.

Brentnall, S. J., D. J. Beerling, C. P. Osborne, M. Harland, J. E. Francis, P. J. Valdes, and V. E. Wittig, 2005: Climatic and ecological determinants of leaf lifespan in polar forests of the high CO2 Cretaceous 'greenhouse' world. *Glob. Change Biol.*, **11**, 2177-2195.

Bugmann, H., 2001: A review of forest gap models. *Climate Change*, **51**, 259-305.

Chambers, J. Q., R. I. Negron-Juarez, D. M. Marra, A. D. Vittorio, J. Tews, D. Roberts, G. H. M. Ribeiro, S. E. Trumbore, and N. Higuchi, 2013: The steady-state mosaic of distrubance and succession across an old-growth Central Amazon forest landscape. *Proc. Natl. Acad. Sci. U.S.A.*, **110**, 3949-3954.

Cox, P., 2001: Description of the "TRIFFID" Dynamic Global Vegetation Model, Met Office, Hadley Centre, Bracknell, United Kingdom, Tech. Note 24, pp.

Curtis, J. T., and M. L. Partch, 1948: Effect of fire on the competition between blue grass and certain prairie plants. *American Midland Naturalist*, **39**, 437-443.

Daufresne, T., and L. O. Hedin, 2005: Plant coexistence depends on ecosystem nutrient cycles: Extension of the resource-ratio theory. *Proc. Natl. Acad. Sci. U.S.A.*, **102**, 9212-9217.

Fernandez-Illescas, C. P., and I. Rodriguez-Iturbe, 2003: Hydrologically driven hierarchical competition - colonization models: the impact of interannual climate fluctuations. *Ecological Monographs*, **73**, 207-222.

Friedl, M., A. Strahler, C. Schaaf, J. C. F. Hodges, and J. Salomon, 2013: Binary MODIS MOD12C1 0.25 Degree Land Cover Climate Modeler Grid. Available at [http://duckwater.bu.edu/lc/] from the Department of Geography, Boston University, Boston, Massachusetts, USA.

Heinl, M., J. Silva, M. Murray-Hudson, and B. Tacheba, 2007: Post-fire succession on savanna habitats in the Okavango Delta wetland, Botswana. *J. Trop. Eco.*, **23**, 705-713.

Hurtt, G. C., L. P. Chini, S. Frolking, R. A. Betts, J. Feddema, G. Fischer, J. P. Fisk, K. Hibbard, R. A. Houghton, A. Janetos, C. D. Jones, G. Kindermann, T. Kinoshita, K. Klein Goldewijk, K. Riahi, E. Shevliakova, S. Smith, E. Stehfest, A. Thomson, P. Thornton, D. P. van Vuuren, and Y. P. Wang, 2011: Harmonization of land-use scenarios for the period 1500-2100: 600 years of global gridded annual land-use transitions, wood harvest, and resulting secondary lands. *Climate Change*, **109**, 117-161.

Johnstone, J. F., F. S. Chapin III, J. Foote, J. Kemmett, K. Price, and L. Viereck, 2004: Decadal observation of tree regeneration following fire in boreal forests. *Can. J. For. Res.*, **34**, 267-273.

Kauffman, E., 2003: Atlas of the biodiversity of California: climate and topography, Number of 12-15 pp

Keeley, J. E., C. J. Fotheringham, and M. Baer-Keeley, 2005: Determinants of postfire recovery and succession in mediterranean-climate shrublands of California. *Ecol. Appl.*, **15**, 1515-1534.

Keeley, S. C., J. E. Keeley, and S. M. Hutchinson, 1981: Postfire succession of the herbaceous flora in southern California chaparral. *Ecology*, **62**, 1608-1621.

Kovaleva, N. M., and G. A. Ivanova, 2013: Recovery of ground vegetation at the initial stage of fire succession. *Contemp. Probl. Ecol.*, **6**, 205-215.

Kramer, P. J., and T. T. Kozlowski, 1979: Physiology of woody plants, Academic press, New York

Kutzbach, J., G. Bonan, J. Foley, and S. P. Harrison, 1996: Vegetation and soil feedbacks on the response of the African monsoon to orbital forcing in the early to middle Holocene. *Nature*, **384**, 623-626.

Latifovic, R., Z. L. Zhu, J. Cihlar, C. Giri, and I. Olthof, 2004: Land cover mapping of North and Central America - Global Land Cover 2000. *Remote Sens. Environ.*, **89**, 116-127.

Li, R., and V. K. Arora, 2012: Effect of mosaic representation of vegetation in land surface schemes on simulated energy and carbon balances. *Biogeoscience*, **9**, 593-605.

Lienard, J., D. Gravel, M. Tallutto, and N. Strigul, 2014: Data-intensive multidimensional modeling of forest dynamics.

Melton, J. R., and V. K. Arora, 2014: Sub-grid scale representation of vegetation in global land surface schemes: implications for estimation of the terrestrial carbon sink. *Biogeoscience*, **11**, 1021-1036.

Melton, J. R., and V. K. Arora, 2016: Competition between plant functional types in the

Canadian Terrestrial Ecosystem Model (CTEM) v. 2.0. *Geosci. Model Dev.*, **accepted**.

Miller, D. J., 1995: Herds on the move: winds of change among pastoralists in the Himalayas and on the Tibetan Plateau, ICIMOD, Kathmandu, Nepal, pp. 27.

Miller, D. J., 2005: The Tibetan Steppe, in: *Grasslands of the world* [Suttie, J. M., Reynolds, S. G., and Batello, C.s (eds.)],FAO, Rome, pp. 495.

Moorcroft, P. R., G. C. Hurtt, and S. W. Pacala, 2001: A method for scaling vegetation dynamics: The ecosystem demography model (ED). *Ecol. Monogr.*, **71**, 557-586.

Omi, P. N., 2005: Forest Fires, ABC-CLIO, Inc., California, 62 pp.

Purves, D., and S. Pacala, 2008: Predictive models of forest dynamics. *Science*, **320**, 1452-1453.

Ramankutty, N., and J. A. Foley, 1999: Estimating historical changes in global land cover: Croplands from 1700 to 1992. *Global Biogeochem. Cyces*, **13**, 997-1027.

Ritchie, T. C., and G. M. MacDonald, 1986: The patterns of post-glacial spread of White Spruce. *J. Biogeogr.*, **13**, 527-540.

Scheiter, S., S. I. Higgins, C. P. Osborne, C. Bradshaw, D. Lunt, B. S. Ripley, L. L. Taylor, and D. J. Beerling, 2012: Fire and fire-adapted vegetation promoted C4 expansion in the late Miocene. *New Phytologist*, **195**, 653-666.

Sitch, S., B. Smith, I. C. Prentice, A. Arneth, A. Bondeau, W. Cramer, J. O. Kaplan, W. Lucht, M. T. Sykes, K. Thonicke, and S. Venevsky, 2003: Evaluation of ecosystem dynamics, plant geography and terrestrial carbon cycling in the LPJ dynamic global vegetation model. *Glob. Change Biol.*, **9**, 161-185.

Stensrud, D. J., 2009: Parameterization sehemes: keys to understanding numerical weather prediction models, Cambride University Press, New York, 459 pp.

Stephenson, N. L., 1998: Actual evapotranspiration and deficit: biologically meaningful correlates of vegetation distribution across spatial scales. *J. Biogeogr.*, **25**, 855-870.

Uhl, C., R. Buschbacher, and E. A. S. Serrao, 1988: Abandoned pastures in eastern Amazonia. I. Patterns of plant succession. *J. Ecology*, **76**, 663-681.

Verseghy, D., 2012: The Canadian land surface scheme, Mannual/Documentation version 3.6, Climate Research Division, Science and Technology Branch, Environmet Canada, pp.

Wang, A., D. T. Price, and V. K. Arora, 2006: Estimating changes in global vegetation cover (1850-2100) for use in climate models. *Global Biogeochem. Cyces*, **20**, GB3028.

Wen, X., G. Tang, S. Wang, and J. Huang, 2011: Comparison of global mean temperature series. *Advances in Climate Change Research*, **2**, 187-192.

Williams, B. P., I. G. Johnston, S. Covshoff, and J. M. Hibberd, 2013: Phenotypic landscape

inference reveals multiple evolutionary paths to C4 photosynthesis. *eLife*, **2**, e00961.

Xiang, S., and Z. Xiaodong, 2014: Investigation of Uncertainties of Estiblishment Schemes in Dynamic Global Vegetation Models. *Adv. Atmos. Sci.*, **31**, 85-94.

Xie, W., X. Cheng-Hua, L. Xian-Wei, and W. Dong-Ju, 2013: Effects of a winter wildfire on plant community structure and forage quality in subalpine grassland of western Sichuan, China. *CJPE*, **37**, 922-932.

Yamori, W., K. Hikosaka, and D. A. Way, 2013: Temperature response of photosynthesis in C3, C4, and CAM plants: temperature acclimation and temeprature adaptation. *Photosynth. Res.*, **119**, 101-117.

Table 1: Plant functional types (PFTs) represented in CTEM and their relation to CLASS PFTs.

| CLASS PFTs | CTEM PFTs | CTEM PFT Symbol |
|---|---|---|
| Needleleaf trees | Needleleaf evergreen trees | NDL-EVG |
| | Needleleaf deciduous trees | NDL-DCD |
| Broadleaf trees | Broadleaf evergreen trees | BDL-EVG |
| | Broadleaf cold deciduous trees | BDL-DCD-CLD |
| | Broadleaf drought/dry deciduous trees | BDL-DCD-DRY |
| Crops | $C_3$ Crop | CROP-C3 |
| | $C_4$ Crop | CROP-C4 |
| Grasses | $C_3$ Grass | GRASS-C3 |
| | $C_4$ Grass | GRASS-C4 |

Table 2 : Root Mean Square Error (RMSE, percentage) for simulated coverages of PFTs between the modelled (using both the composite and mosaic configurations) and the observation-based modified WANG06 estimates, heterogeneity index (dimensionless fraction) for modelled values for the composite and mosaic configurations, and root mean square difference (RMSD, percentage) for simulated coverages of PFTs between the composite and mosaic approaches.

The lowest value of the RMSE, for each site, for composite or mosaic approach is underlined. Since RMSE is bigger than RMSD for all sites, the results imply that the modelled results from the composite and mosaic approaches are closer to each other than to observations-based estimate. In addition, RMSD is generally higher when the heterogeneity index is higher, indicating that the modelled fractional coverages of PFTs are more different in the composite and mosaic configurations when more PFTs exist in a grid cell and the land cover is more heterogeneous.

| **Location** | **RMSE** | | **Heterogeneity index** | | **RMSD** |
|---|---|---|---|---|---|
| | **Composite** | **Mosaic** | **Composite** | **Mosaic** | |
| Amazon | 2.3% | 2.5% | 0.11 | 0.12 | 0.4% |
| India | 12.5% | 7.6% | 0.92 | 0.89 | 5.1% |
| South Sudan | 10.3% | 16.2% | 0.87 | 0.71 | 9.9% |
| California | 10.2% | 13.5% | 0.72 | 0.62 | 6.2% |
| Vancouver Island | 6.5% | 5.6% | 0.24 | 0.20 | 0.8% |
| Siberia | 18.4% | 20.2% | 0.70 | 0.66 | 2.2% |
| Tibetan Plateau | 2.2% | 1.2% | 0.34 | 0.37 | 1.1% |
| **Average (all sites)** | **9.0%** | **9.6%** | | | **3.7%** |

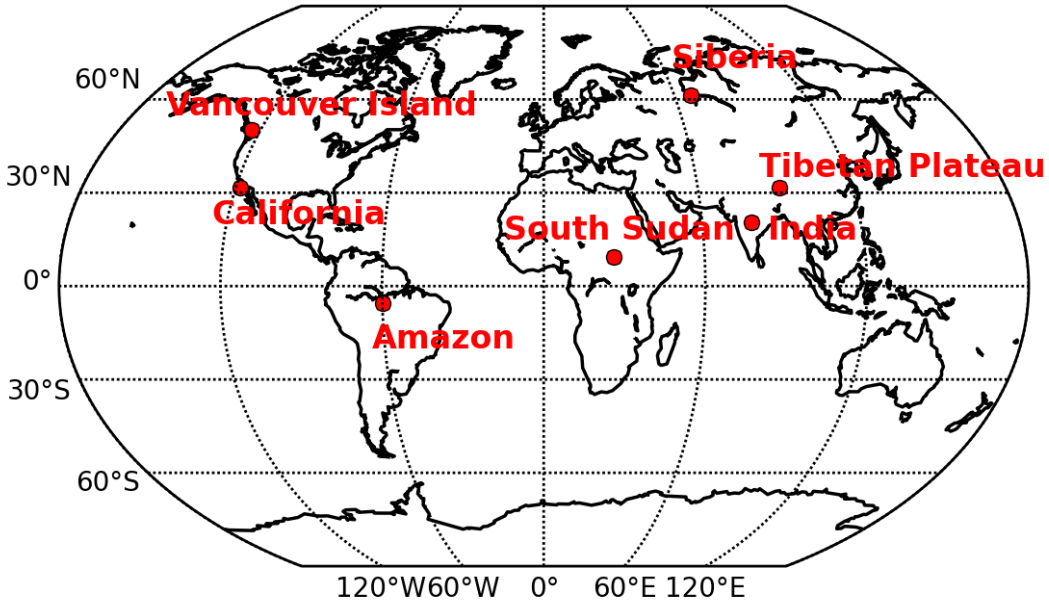


Figure 1. Location map of the study sites for which the competition parameterization of the CLASS-CTEM modelling framework is evaluated.

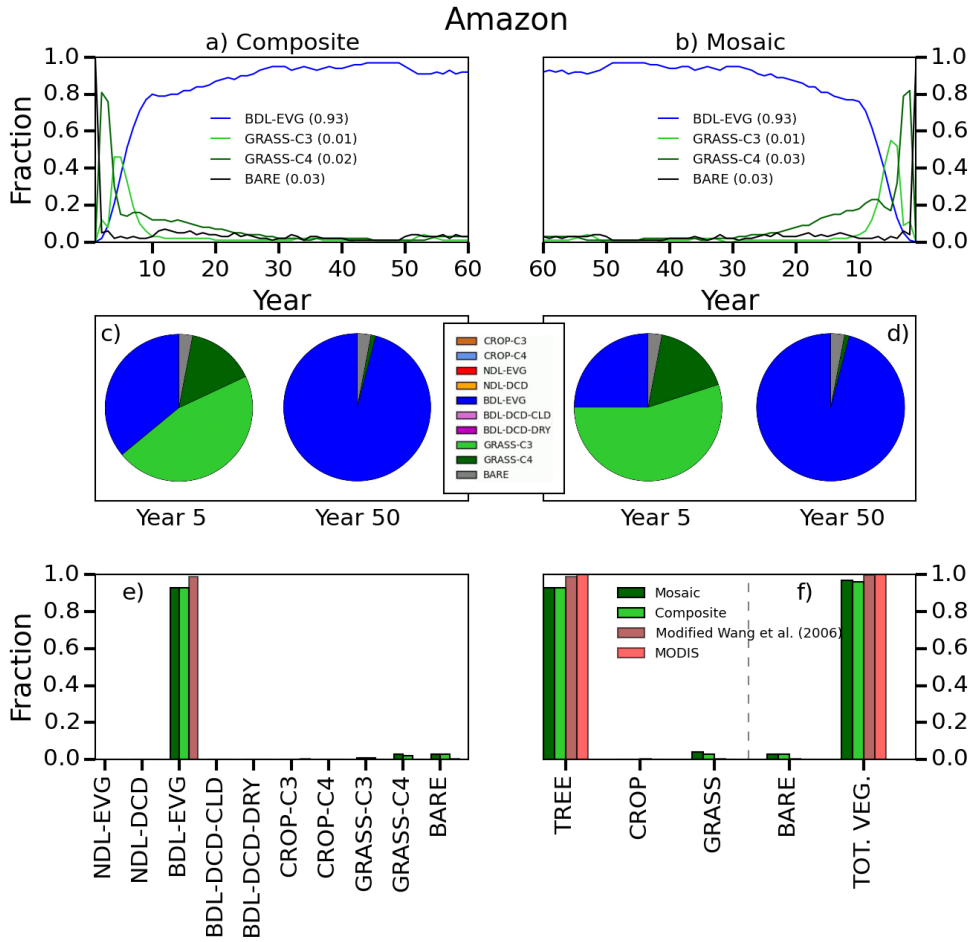


Figure 2. Evolution of CLASS-CTEM simulated fractional coverage of PFTs in the a) composite and b) b) mosaic configurations, during the first 60 years (out of 400 simulated years) at the Amazon location. The values printed in the legend parenthesis are mean over the last 40 years (when PFTs fractions exhibit equilibrium). Note that in panel b for the mosaic configuration the x-axis is reversed for easier comparison of simulated fractional coverages between the two approaches. Panel c) and d) show the snapshot of simulated fractional coverages of model PFTs at year 5 and 50 for the composite and mosaic configurations, respectively. Panel e) compares the fractional coverage of simulated individual PFTs with the observation-based modified WANG06 product and panel f) compares simulated tree-grass-bare and total vegetated fractions with the observation-based modified WANG06 and MODIS products.

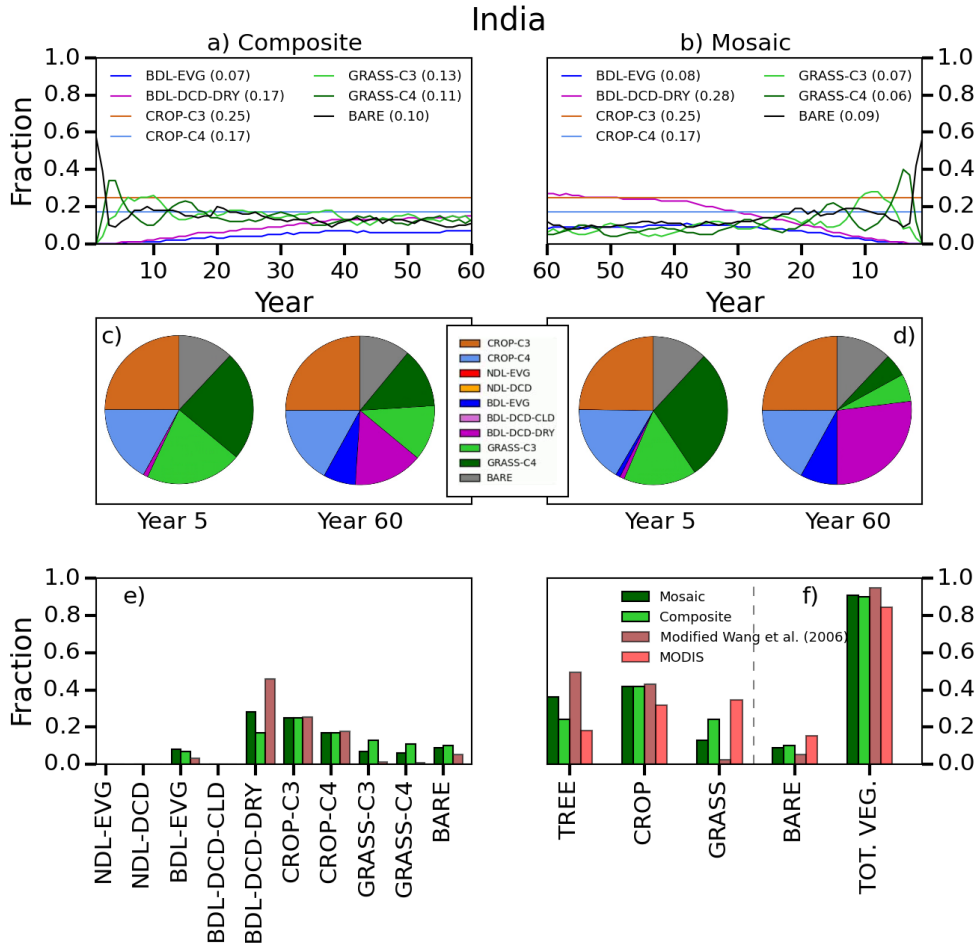


Figure 3: Evolution of CLASS-CTEM simulated fractional coverage of PFTs in the a) composite and b) b) mosaic configurations, during the first 60 years (out of 400 simulated years) at the location in India. The values printed in the legend parenthesis are mean over the last 40 years (when PFTs fractions exhibit equilibrium). Note that in panel b for the mosaic configuration the x-axis is reversed for easier comparison of simulated fractional coverages between the two approaches. Panel c) and d) show the snapshot of simulated fractional coverages of model PFTs at year 5 and 60 for the composite and mosaic configurations, respectively. Panel e) compares the fractional coverage of simulated individual PFTs with the observation-based modified WANG06 product and panel f) compares simulated tree-grass-bare and total vegetated fractions with the observation-based modified WANG06 and MODIS products.

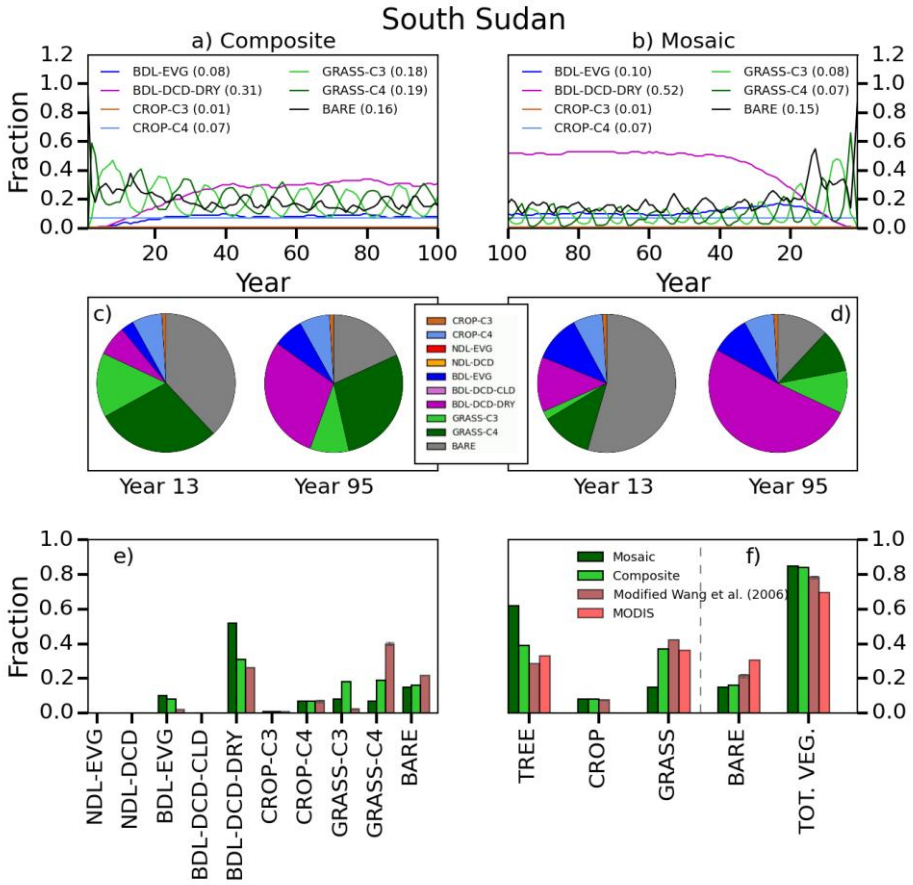


Figure 4: Evolution of CLASS-CTEM simulated fractional coverage of PFTs in the a) composite and b) b) mosaic configurations, during the first 100 years (out of 400 simulated years) at the location in South Sudan. The values printed in the legend parenthesis are mean over the last 40 years (when PFTs fractions exhibit equilibrium). Note that in panel b for the mosaic configuration the x-axis is reversed for easier comparison of simulated fractional coverages between the two approaches. Panel c) and d) show the snapshot of simulated fractional coverages of model PFTs at year 13 and 95 for the composite and mosaic configurations, respectively. Panel e) compares the fractional coverage of simulated individual PFTs with the observation-based modified WANG06 product and panel f) compares simulated tree-grass-bare and total vegetated fractions with the observation-based modified WANG06 and MODIS products.

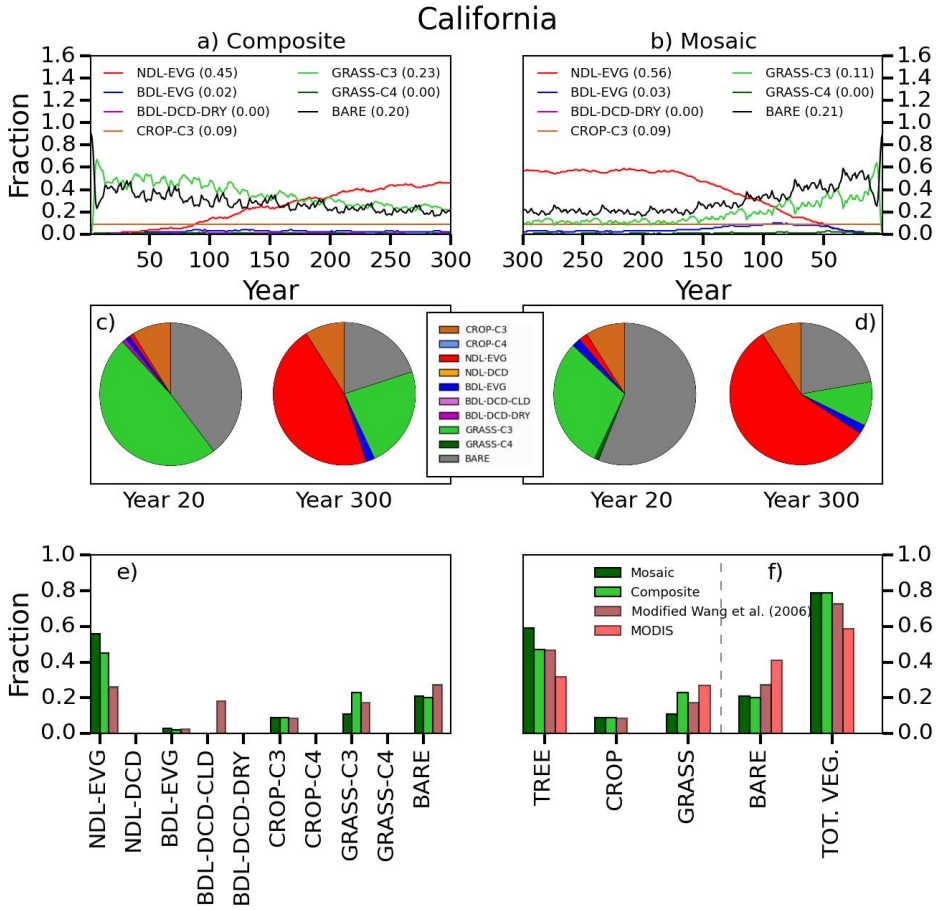


Figure 5: Evolution of CLASS-CTEM simulated fractional coverage of PFTs in the a) composite and b) b) mosaic configurations, during the first 300 years (out of 400 simulated years) at the California location. The values printed in the legend parenthesis are mean over the last 40 years (when PFTs fractions exhibit equilibrium). Note that in panel b for the mosaic configuration the x-axis is reversed for easier comparison of simulated fractional coverages between the two approaches. Panel c) and d) show the snapshot of simulated fractional coverages of model PFTs at year 20 and 300 for the composite and mosaic configurations, respectively. Panel e) compares the fractional coverage of simulated individual PFTs with the observation-based modified WANG06 product and panel f) compares simulated tree-grass-bare and total vegetated fractions with the observation-based modified WANG06 and MODIS products.

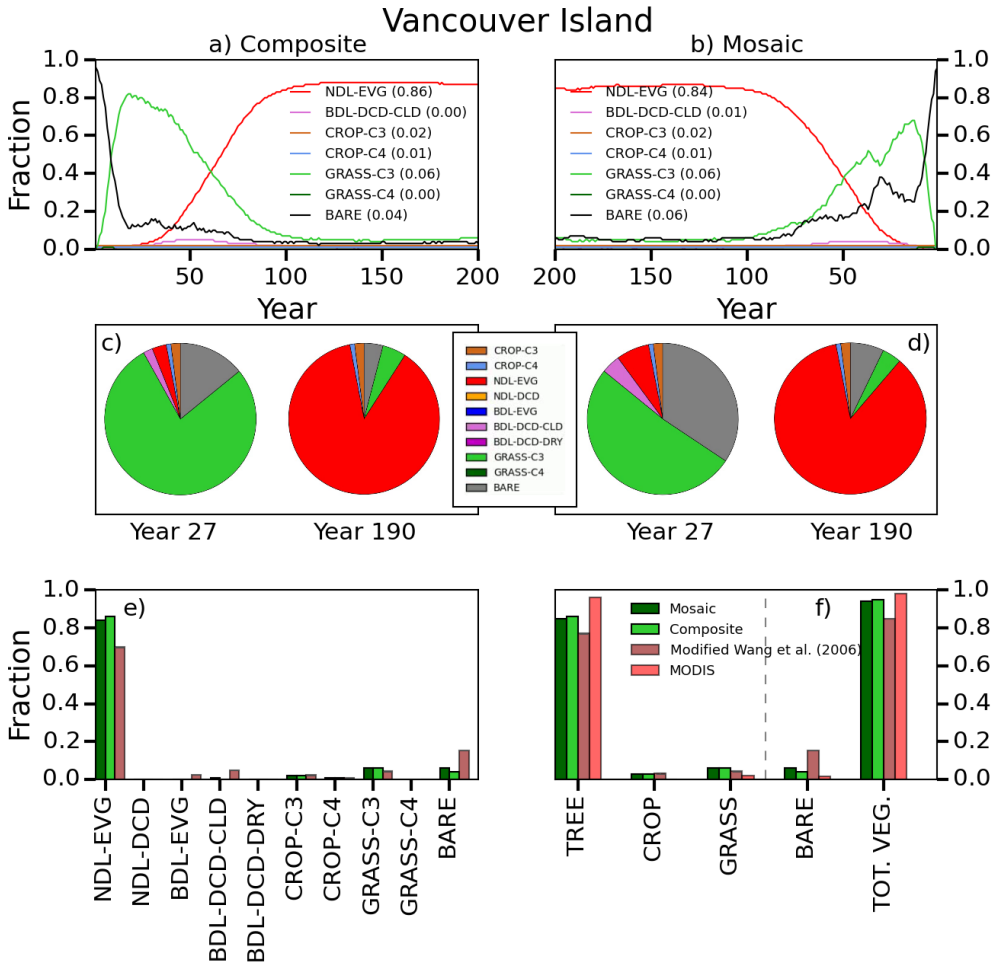


Figure 6: Evolution of CLASS-CTEM simulated fractional coverage of PFTs in the a) composite and b) b) mosaic configurations, during the first 200 years (out of 400 simulated years) at the Vancouver Island location in Canada. The values printed in the legend parenthesis are mean over the last 40 years (when PFTs fractions exhibit equilibrium). Note that in panel b for the mosaic configuration the x-axis is reversed for easier comparison of simulated fractional coverages between the two approaches. Panel c) and d) show the snapshot of simulated fractional coverages of model PFTs at year 27 and 190 for the composite and mosaic configurations, respectively. Panel e) compares the fractional coverage of simulated individual PFTs with the observation-based modified WANG06 product and panel f) compares simulated tree-grass-bare and total vegetated fractions with the observation-based modified WANG06 and MODIS products.

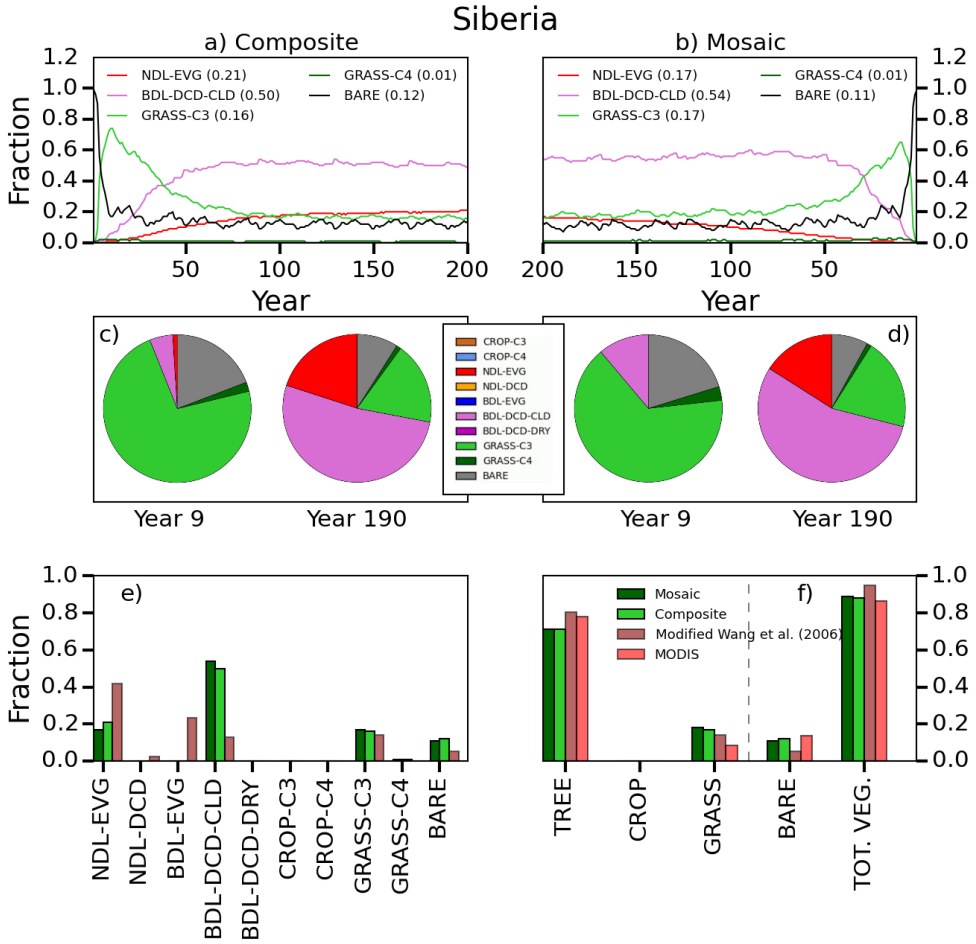


Figure 7: Evolution of CLASS-CTEM simulated fractional coverage of PFTs in the a) composite and b) b) mosaic configurations, during the first 200 years (out of 400 simulated years) at the Siberia location. The values printed in the legend parenthesis are mean over the last 40 years (when PFTs fractions exhibit equilibrium). Note that in panel b for the mosaic configuration the x-axis is reversed for easier comparison of simulated fractional coverages between the two approaches. Panel c) and d) show the snapshot of simulated fractional coverages of model PFTs at year 9 and 190 for the composite and mosaic configurations, respectively. Panel e) compares the fractional coverage of simulated individual PFTs with the observation-based modified WANG06 product and panel f) compares simulated tree-grass-bare and total vegetated fractions with the observation-based modified WANG06 and MODIS products.

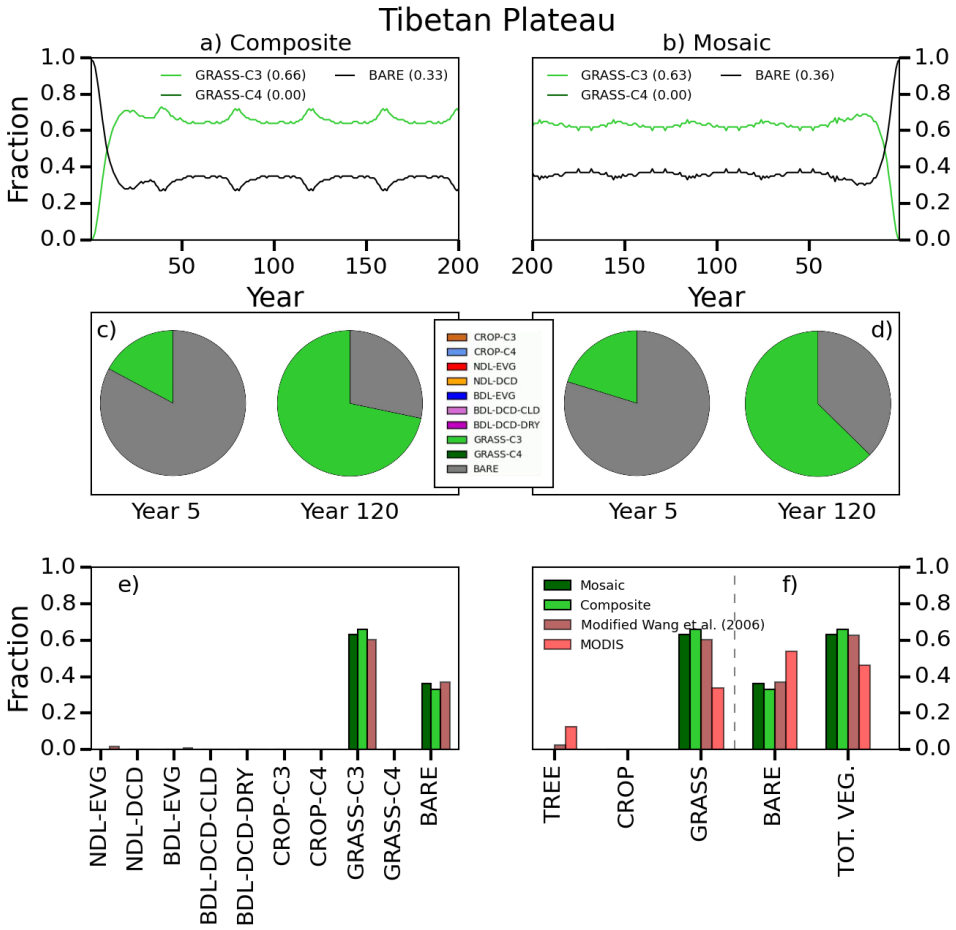


*Figure 8:* Evolution of CLASS-CTEM simulated fractional coverage of PFTs in the a) composite and b) b) mosaic configurations, during the first 200 years (out of 400 simulated years) at the Tibetan Plateau location. The values printed in the legend parenthesis are mean over the last 40 years (when PFTs fractions exhibit equilibrium). Note that in panel b for the mosaic configuration the x-axis is reversed for easier comparison of simulated fractional coverages between the two approaches. Panel c) and d) show the snapshot of simulated fractional coverages of model PFTs at year 5 and 120 for the composite and mosaic configurations, respectively. Panel e) compares the fractional coverage of simulated individual PFTs with the observation-based modified WANG06 product and panel f) compares simulated tree-grass-bare and total vegetated fractions with the observation-based modified WANG06 and MODIS products.